Research Article

Nano Biomed Eng

Green Synthesis of Indole-pyrazole-capped Cadmium Sulphide Quantum Dots and Evaluation of Their Cytotoxicity Activity and Protein Interaction

Senzekile Majola, Myalowenkosi Sabela, Robert M. Gengan, Talent R. Makhanya
Department of Chemistry, Durban University of Technology, P.O Box 1334, Durban 4000, South Africa

Corresponding author. Email: myalos@dut.ac.za

Received: Jan. 17, 2024; **Revised:** Mar. 5, 2024; **Accepted:** Mar. 25, 2024

Citation: S. Majola, M. Sabela, R.M. Gengan, et al. Green synthesis of indole-pyrazole-capped cadmium sulphide quantum dots and evaluation of their cytotoxicity activity and protein interaction. *Nano Biomedicine and Engineering*, 2024, 16(3): 460−472.
http://doi.org/10.26599/NBE.2024.9290077

Abstract

Plant extracts play an essential role in bioreducing metal ions and capping the resultant nanomaterials. We report the green synthesis of indole pyrazole-capped cadmium sulfide quantum dots (TRPIDC-CH_3CdSQDs) using *Moringa oleifera* leaf extract and indole pyrazole ligand. Morphological analysis using a high-resolution electron microscope indicated the presence of spherical particles with an average diameter of 4.5 nm. The ultraviolet–visible (UV–Vis) spectroscopy results exhibited a bandgap energy of 2.95 eV, and phytochemical deposition on the TRPIDC-CH_3CdSQDs was confirmed by Fourier transform infrared (FTIR). The cytotoxicity analysis was conducted using the 3-(4,5)-dimethylthiahiazo(-z-y1)-3,5-di-phenytetrazoliumromide (MTT) assay on two cancer ((breast (MCF-7) and lung (A549)) cells and a normal human embryonic kidney (HEK293) cell. Low cytotoxic activity was found for TRPIDC-CH_3CdSQDs against all three cell types, the highest activity percentage being 63.80% against MCF-7 and TRPIDC-CH_3CdSQDs show a dose-dependent increase in cytotoxic activity. Spectroscopic interaction studies were undertaken with human serum albumin using UV–Vis and fluorescence spectroscopy. The interactions between TRPIDC-CH_3CdSQDs and human serum albumin were hydrophobic. Using corrected fluorescence data, the Stern–Volmer constant and binding constant were 2.06×10^3 and 2.85×10^3 mol·L^{-1}, respectively. The findings indicate its potential to be used in drug delivery.

Keywords: pyrazole-capped CdSQDs; *Moringa oleifera* leaf extract; MTT assay; drug delivery; human serum albumin (HSA)

Introduction

Developing a clean synthetic approach ("green chemistry") to obtain desired nanomaterials for different biomedical applications is essential to promoting its clinical transformation. An environmentally acceptable solvent system and eco-friendly reducing and capping agents are important features of "green" synthesis [1, 2]. Eco-friendly synthetic techniques are becoming popular as a result of the demand for greener approaches to counteract the high costs and higher energy requirements of chemical and physical methods. Hence, scientists continue to search for cheaper synthesis methods. The three main concepts for preparing nanomaterials in a green synthesis approach are the choice of the solvent medium (preferably water), an environmentally friendly reducing agent, and a nontoxic material to

stabilize the nanomaterials [3]. Plant extracts are a primary source of many biologically active compounds that are essentially used in pharmaceutical, agricultural, and cosmetic industries [4]. They reduce metal ions from their surface and their metabolites, such as sugars, alkaloids, terpenoids, phenolic acids, polyphenols, flavonoids, and proteins. They also play a vital role in bioreducing metal ions and capping the resulting nanomaterials [5].

The green synthesis of plant-extracted nanomaterials has emerged massively due to the ability of natural products to reduce nanomaterial cytotoxicity [6, 7]. Physical and chemical approaches to synthesize nanomaterials they require dangerous reducing agents, such as sodium borohydride or hydrazine, which also contain unsafe by-products. Greener routes can reduce environmental impact and counteract higher cost and energy requirements of chemical and physical methods [7]. This study used *Moringa oleifera* leaves to synthesize quantum dots (QDs). *M. oleifera*, also known as horseradish tree, drumstick tree, or tree of life, belongs to the family Moringaceae. It is a drought-resistant tree native to the Indian sub-Himalayan regions and it is the most cultivated species of the Moringaceae family [8]. Almost all parts of this tree are useful: the trunk is used to produce gums, leaves as forage, nectar flowers in honey, and powdered seeds for water purification [8, 9]. Its leaf extract has several properties, including antioxidant, anti-inflammatory, anticancer, antifungal, and hypotensive activities [10, 11]. *M. oleifera* contains tannins, steroids, triterpenoids, flavonoids, saponins, and alkaloids that are natural alternative reducing agents for nanomaterial synthesis [12]. Other researchers have reported the use of *M. oleifera* leaves [13–15] and seeds [14, 16] to synthesize various nanomaterials.

QDs are 2–10 nm long semiconductor nanoparticles with three dimensions. Compared with conventional organic and inorganic fluorophores (e.g., organic dyes and fluorescent proteins), they have unique optical and electronic properties, such as wide and continuous absorption spectra, size-dependent optical, and high light stability [17, 18]. Based on their unique characteristics, QDs have gained significant attention in biomedical imaging, DNA detection, immunoassay, drug delivery, solar energy generation, and electronic industries [18]. Plants [6, 7], microorganisms [19, 20], and proteins [21] have been used to produce metal-based QDs, resulting in increased functionality and biocompatibility. These materials aid in the biological creation of QDs by influencing nanocrystal nucleation, morphology, surface properties, and size constraints within cells. However, stability, quantification, and increasing product yield are challenging. Factors like extract and salt concentrations, pH, temperature, solvent, and reaction time can be optimized to improve QD quality and quantity. To generate a suitable surface structure with long-term stability, the bare QDs must be modified with various ligands. Additionally, green synthesized nanomaterials are relatively unstable compared to physical and chemical methods; therefore, new stabilizing agents are required [22–24].

In this work, cadmium sulfide QDs (CdSQDs) were capped with indole pyrazole ligands to enhance their stability [25]. Obtaining novel compounds is becoming more and more popular, particularly heterocyclic chemicals that may provide alternative biological activity pathways to potentially overcome drug resistance. Pyrazoles are five-membered aromatic heterocycles containing two adjacent nitrogen atoms; they act as pharmacophores in various molecular entities and are available from natural sources. However, synthetic molecules dominate the pharmaceutical industry due to the high yield and purity obtained from the basic substrate [26]. Pyrazoles are a good template for designing and developing diverse ligands because they can enhance numerous biological properties, such as anti-hyperglycemic, analgesic, and anti-inflammatory properties [25]. Furthermore, they enable the attachment of biomolecules, such as enzymes and proteins. This study focused on synthesizing QDs via a rapid, cost effective, and environmentally friendly plant-based green approach. Nanomaterials with low toxicity and environmental impact are crucial in real-world biomedical applications. Therefore, their cytotoxic activity will be assessed using MCF-7, A549, and HEK293 cells. Their protein interactions with human serum albumin (HSA) will also be evaluated to assess their potential in biological applications, such as drug delivery.

Experimental

Chemicals and reagents

M. oleifera leaves were collected from a nearby suburb (Phoenix) in Durban, South Africa. Potassium

dihydrogen phosphate (KH_2PO_4), dipotassium hydrogen phosphate (K_2HPO_4), cadmium sulfate ($CdSO_4$, ≥ 99.99% purity), sodium sulfide (Na_2S, ≥ 98% purity), HSA lyophilized powder (≥ 97% purity), Folin–Ciocalteu reagent (FCR), tannic acid, bromocresol green, atropine, chloroform, and quercetin were purchased from Sigma Aldrich (South Africa). The human embryonic kidney cells (HEK293), breast cancer cells (MC-7), lung cancer cells (A549), Dulbecco's modified eagle medium (DMEM), and 3-(4,5)-dimethylthiahiazo(-z-y1)-3,5-di-phenytetrazoliumromide (MTT) were purchased from Sigma Aldrich (USA). Indole pyrazole (TRPIDC-CH_3) ligand was synthesized by one of our coauthors at the green synthesis laboratory (Durban University of Technology, South Africa) [25].

Apparatus

The technology used to characterize the synthesized QDs includes the Agilent Cary 60 ultraviolet–visible (UV–Vis) spectrophotometer, Agilent Cary 630 Fourier transform infrared (FTIR) spectrometer, and a high-resolution electron microscope (HR-TEM; model JEM 2100 fitted with a Max Oxford LaB_6 emitter). The MTT assay was conducted in 96-well, flat-bottom microtiter plates (Costar, Corning, USA). The spectroscopic investigations on the interaction between nanomaterials and proteins were performed using FTIR, UV–Vis, and Varian Cary Eclipse fluorescence spectrophotometer. The pH/ion meter coupled to a stirrer (Hannan Instruments Microprocessor) was used to adjust the pH of the buffer solutions. Buffers and designated samples were stored at 4°C, and all analytical measurements were performed at room temperature.

Qualitative determination of phytochemicals (*M. oleifera* leaf extract)

Allium sativum extraction

M. oleifera leaves were washed with deionized water and then air-dried. Precisely 3.0 g of leaves were added to 30 mL of methanol and incubated in the dark for 24 h at room temperature. Next, the leaf extract was filtered through Whatman No.1 filter paper and stored at 4 °C for further use.

Alkaloids

2.0 mL of extract was added in 3.0 mL of 2% (*v*/*v*) HCl, and 3–5 drops of Mayer's reagent were added [27]. The presence of alkaloids was evaluated by monitoring the appearance of a dull white precipitate.

Flavonoids

3.0 mL of extract was treated with a few drops of ferric chloride solution. The change in color was monitored for the presence of flavonoids [27].

Terpenoids

The test was conducted by mixing 3.0 mL of the extract with 2 mL of chloroform in a test tube. Next, 2 mL of concentrated H_2SO_4 was added gently. The presence of terpenoids was indicated by the formation of a reddish-brown precipitate [27].

Quantitative determination of phytochemicals (*M. oleifera* leaf extract)

Phenols

The FCR technique was used to determine the phenolic content of the extract [28]. Phenols in the extracts reduce FCR, resulting in the formation of a blue color that darkens with increasing phenolic content. The solution was covered and left at room temperature in a dark cupboard for 5 min. Next, 1.5 mL of 5% Na_2CO_3 was added, well combined, and the mixture was allowed to stand at room temperature for 2 hrs in a dark area. The absorbances were measured at 750 nm. Tannic acid was prepared at various concentrations (5, 10, 25, 50, 75, 100, 150, and 200 μg·mL^{-1}) to plot the standard curve, and the amount of phenol in the extract was calculated using the milligrams (mgTAE·g^{-1}) of equivalent tannic acid. The assay was conducted in triplicate.

Flavonoids

The flavonoid concentration was determined using the aluminum chloride colorimetric method [28]. Quercetin (1 mg·mL^{-1}) was prepared in different concentrations (10, 50, 75, 100, 150, 200, 250, and 300 μg·mL^{-1}) and used as a reference. 1 mL of quercetin or extract was combined with 0.3 mL of 5% sodium nitrite. The solution was then incubated for 5 min at room temperature. Thereafter, 0.3 mL of 10% aluminum chloride was added, and the solution was once again allowed to stand for 5 min at room temperature. The solution was then combined with 2 mL of 1 mol·L^{-1} NaOH and left to stand at room temperature for an additional 10 min. After measuring the absorbance at 510 nm, the flavonoid concentration was expressed as milligrams of quercetin equivalent per gram of extract (mgQE·g^{-1}). This assay was done

in triplicate.

Alkaloids

A solution of bromocresol green (BCG) was used for this test [28]. BCG (23 mg), 0.67 mol/L NaOH (3 mL), and distilled water (5 mL) were combined to create a fresh bromocresol solution. The resultant solution was then diluted and brought up to 300 mL using distilled water. An atropine reference solution (0.05 mg·mL^{-1}) was prepared with distilled water and diluted to 10, 50, 75, 100, 150, 200, 250, and 300 µg·mL^{-1}. To extract the alkaloids, 1 mL of the extract and 1 mL of standard (at varying concentrations) were added independently to 5 mL of the bromocresol green solution and 5 mL of the phosphate buffer (pH 4.7). Subsequently, 4 mL of chloroform was added and shaken vigorously. Thus, a BCG–chloroform complex was created, and the resulting chloroform fraction was gathered and placed in a test tube. Next, the absorbance at 470 nm was measured. The unit of measurement for the total alkaloid content was milligrams of atropine equivalent per gram of extract (mgAE·g^{-1}). The test was made in triplicate.

Indole pyrazol-capped CdSQDs synthesis

The indole pyrazol (TRPIDC-CH_3)-capped CdSQDs synthesis was performed according to the method described by Shivaji et al., with minor modifications [29]. Approximately 2.0 mL of 0.025 mol·L^{-1} of cadmium sulfate ($CdSO_4$) and 2.0 mL of ligand (TRPIDC-CH_3) solutions were added to 30 mL of the filtered leaf extract and incubated for 3 days in the dark. The TRPIDC-CH_3 solution was prepared by dissolving the ligand in 10% DMSO. After 3 days of incubation, 0.5 mL of 0.025 mol·L^{-1} sodium sulfide (Na_2S) was added and incubated for another 4 days to produce TRPIDC-CH_3CdSQDs. The color change from bottle green to bright yellow indicates TRPIDC-CH_3CdSQDs formation [29]. The schematic diagram for the plant extract preparation and TRPIDC-CH_3CdSQD synthesis is displayed in Fig. 1.

Cytotoxicity studies with MTT Assay

The MTT assay was conducted in 96-well, flat-bottom microtiter plates (Costar, Corning, USA). The MTT assay used doxorubicin as a standard to determine the rate of cell proliferation as a function of the mitochondrial reduction of tetrazolium salt. The synthesized QDs were tested for anticancer activity against two cancer cell lines, breast (MCF-7) and lung (A549), and normal human embryonic kidney (HEK293) cell lines. Different concentrations (50 and 100 µg·mL^{-1}) of A1-A6 QDs were evaluated in triplicate for 48 h, and the results are expressed as the average ± standard deviation (SD). An aliquot of 90 µL (1 × 10^4 cells) of the MCF-7, A549, and HEK293 cell suspensions was transferred to the microtiter plates. Sterile distilled water was added to the outer wells to prevent medium evaporation. The plates were incubated in a 37 °C humidified incubator for 24 h to allow the cells to attach to the wells. An aliquot of 10 µL of the test QDs was added to the wells at two concentrations (100 and 50 µg·mL^{-1}).

In control wells, 10 µL of dimethyl sulfoxide (DMSO) (1%), DMEM (medium control), and doxorubicin were added. The plates were incubated at 37 °C for 48 h in a humidified incubator with 5%

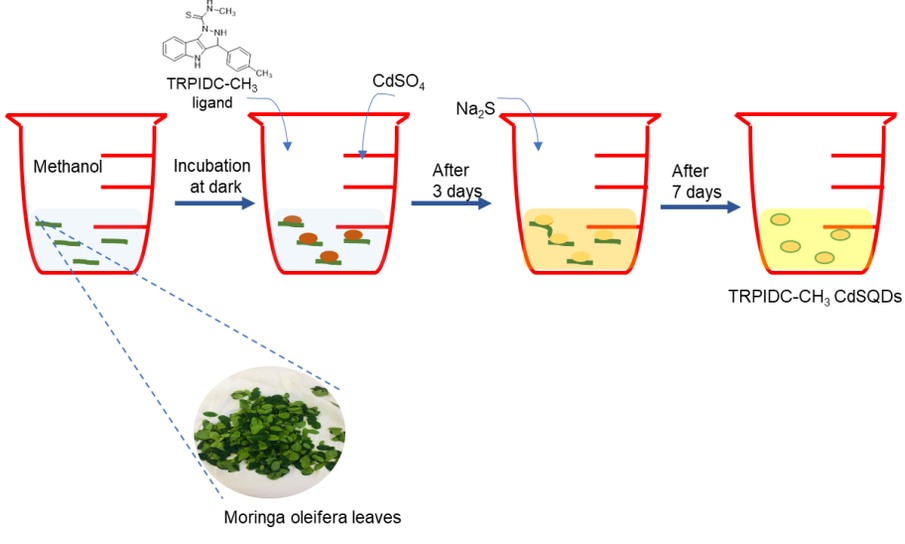

Fig. 1 Schematic diagram for the plant extract preparation and TRPIDC-CH_3 CdSQD synthesis.

CO_2. After incubation, 10 μL of MTT reagent (Sigma, St Louis, USA) was added to the plates, which were incubated for 4 h at 37 °C in a humidified incubator with 5% CO_2. After incubation, 100 μL of DMSO was added to the wells, and the plates were incubated for an additional 1 h. DMSO was added to dissolve the insoluble formazan crystals that are formed by the MTT reagent once they enter the cells. The plates' absorbance was recorded at 590 nm on an ELISA microplate reader (Digital Analogue Systems, Italy) [30, 31]. The cytotoxicity percentage was determined as the difference in percent cell vitality, calculated as the absorbance of the treated cells. Each experiment was performed in triplicate, and the data are presented as mean ± SD. The statistical significance of differences between the groups was analyzed using a one-way ANOVA test followed by a posthoc Bonferroni's test ($p < 0.05$).

Protein interaction studies

Interaction of TRPIDC-CH_3Se NPs with HSA

HSA was dissolved in a phosphate buffer (0.10 mol/L, pH 7.3) and stored in the dark at 4 °C for further use. 50 μL of HSA stock solutions was added to 2.0 mL centrifuge tubes. Varying volumes (0–30 μL) of nanomaterials were successively added (Table 1), topped up with PBS. All test solutions were incubated for 40 min at 37 °C before each measurement, and the interaction between HSA and the nanomaterials was monitored using UV–Vis spectroscopy and FTIR.

UV–Vis absorption studies

The UV–Vis measurements were studied using the following equation [32]:

$$\frac{1}{A_0 - A} = \frac{1}{A_c - A_0} + \frac{1}{A_c - A} \times \frac{1}{K_b [Q]} \quad (1)$$

where A is the HSA absorbance at different nanoparticle concentrations, A_0 is the absorbance of HSA alone, and A_C is the absorbance of the HSA–nanoparticles complex. $[Q]$ is the nanoparticle concentration. The binding constant (K_b) is determined from the slope of the plot of $\frac{1}{(A_0 - A)}$ vs. $\frac{1}{[Q]}$

Fluorescence quenching studies

Fluorescence was measured by exciting HSA at 280 nm, and the emission spectrum was measured at 290–450 nm. Tryptophan fluorescence is used as a probe of the local environment in a protein to determine its structure, dynamics, and ligand binding. The change in the fluorescence intensity at a particular wavelength was analyzed according to the Stern−Volmer equation [33]:

$$\frac{F_0}{F} = 1 + K_{SV}[Q] = 1 + K_q \tau_o [Q] \quad (2a)$$

$$\log\left[\left(\frac{F_0 - F}{F}\right)\right] = \log K_b + n \log[Q] \quad (2b)$$

where F_0 and F are the HSA fluorescence intensities in the absence and presence of the quencher $[Q]$, respectively. K_{SV} is the Stern–Volmer quenching constant, K_q is the bimolecular quenching constant, and τ_0 is the lifetime of the fluorophore in the absence of the quencher (~ 10^{-8} s). K_b is the binding constant, and n is the number of binding sites.

Mode of binding

The thermodynamic parameter change in enthalpy (ΔH) and entropy (ΔS) were determined after measuring K_b at different temperatures, and the results were analyzed according to van't Hoff equation:

$$\ln(K_b) = -\left(\frac{\Delta H}{T}\right) + \left(\frac{\Delta S}{R}\right) \quad (3)$$

where R (8.314 J·mol^{-1}·K^{-1}) and T represent the

Table 1 Volumes of HSA, TRPIDC-CH_3CdSQDs, and PBS used for interaction studies

Mixture No.	Volume of HSA (μL)	Volume of TRPIDC-CH_3CdSQDs (μL)	Volume of phosphate buffer (μL)	Total volume(μL)
1	50	0	1 950	2 000
2	50	5	1 945	2 000
3	50	10	1 940	2 000
4	50	15	1 935	2 000
5	50	20	1 930	2 000
6	50	25	1 925	2 000
7	50	30	1 920	2 000

universal gas constant and absolute temperature, respectively. For hydrogen bonding or van der Waals interactions, ΔH and ΔS are negative; for hydrophobic interactions, ΔH and ΔS are positive; and for electrostatic interactions, ΔH is positive or negative, and ΔS is positive [32]. The change in Gibbs free energy (ΔG) can be further determined from separate terms of enthalpy change (ΔH) and entropy change (ΔS) according to the following equation:

$$\Delta G = -RT \ln K_b = \Delta H - T\Delta S \quad (4)$$

The positive sign of ΔH and negative sign of ΔG indicate that the binding process is endothermic and spontaneous, and the negative sign of ΔH and ΔG indicates that the binding process is exothermic and spontaneous [34].

Results and Discussion

Qualitative determination of phytochemicals (*M. oleifera* leaf extract)

In green synthesis, nanomaterials are mainly affected by the natural phytochemicals existing in the plant extract [35]. A phytochemical screening test of the *M. oleifera* leaf extract that was used to synthesize TRPIDC-CH_3CdSQDs was performed to find out which phytochemicals were present. *M. oleifera* leaves are reported to contain tannins, terpenoids, flavonoids, saponins, and alkaloids [12, 36], which may influence the reduction process and the stability of the synthesized TRPIDC-CH_3CdSQDs. The leaf extract tested positive for flavonoids, alkaloids, and terpenoids, agreeing with the FTIR results (Fig. 2(b)) and the literature (Table 2).

Quantitative determination of phytochemicals (*M. oleifera* leaf extract)

The quantitative determination of the phytochemical content (phenol, flavonoids, and alkaloids) in the leaf extract of *M. oleifera* was conducted using the Agilent Cary 60 UV–Vis spectrophotometer at different wavelengths. The phenolic content was evaluated using a colorimetric reduction-based approach with the FCR and tannic acid as a reference standard, while the flavonoid content was assessed using the aluminum chloride method and quercetin as a reference standard. To calculate the amounts, extrapolation was used to create calibration curves for phenols and flavonoids. The calibration curve for phenols was prepared using the tannic acid concentration, and the amounts were expressed in mg per gram of tannic acid (TAE) equivalency, while the calibration curve for flavonoids was prepared using the quercetin concentration. Results are displayed in Table 3. The estimation of alkaloids was based on the reaction between alkaloids and BCG. A yellow-colored complex with maximum absorption was formed. This complex was fully extractable with chloroform at pH 4.7. A calibration curve was created for different atropine concentrations and expressed in mg of the equivalent of atropine (A) per gram. The results are also presented in Table 3.

Characterization of biosynthesized TRPIDC-CH_3CdSQDs

The green approach was used to synthesize TRPIDC-CH_3CdSQDs from $CdSO_4$ using methanolic *M. oleifera* leaf extract as an efficient reducing agent and TRPIDC-CH_3 ligand as a stabilizing agent. The dark green solution was incubated in the dark for 7 days, and the solution changed to yellow, suggesting the development of TRPIC-CH_3CdSQDs. This was in agreement with the report from other authors who used tea leaf extract [29], fruit sap of *Opuntia ficus* indica [40], and fungus [17], respectively.

UV–Vis spectroscopy

Figure 2(a) illustrates the TRPIDC-CH_3CdSQDs energy absorption spectrum to show the distinctive energy absorption edge. The absorption band of QDs shifted to a shorter wavelength. The "blue shift" indicates a reduction in size and the formation of QDs [40]. The synthesized TRPIDC-CH_3CdSQDs are within the well-known quantum-confined size range for CdSQDs reported by Shivaji et al. and Kandasamy et al., with an absorption spectrum maximum at 420 nm and a bandgap energy of 2.95 eV [29, 40].

FTIR spectroscopy

Based on the FTIR results in Fig. 2(b) (pink line), the biomolecules of *M. oleifera* leaf extract involved in the bioreduction of QDs mainly are O–H, C=C, and C–H functional groups, which agree with phytochemical screening [37, 41]. The FTIR spectrum of the TRPIDC-CH_3CdSQDs is displayed in Fig. 2(b) (violet line), which gives information about the functional groups involved in reducing cadmium ions and detects some possible biomolecules that are

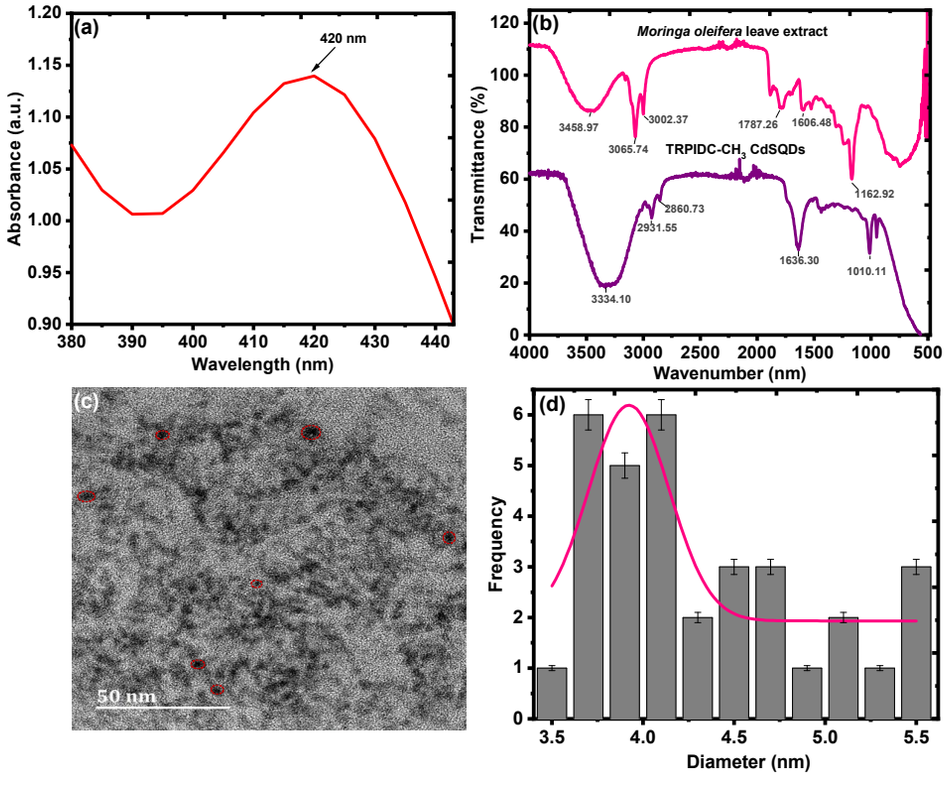

Fig. 2 (a) UV–Vis spectrum of TRPIDC-CH_3CdSQDs, **(b)** FTIR spectrum of TRPIDC-CH_3CdSQDs, **(c)** HR-TEM image of TRPIDC-CH_3CdSQDs, and **(d)** size distribution histogram prepared by Image J software.

capped on QDs. The broadband at 3 458.92 cm^{-1} shifted to 3 334.10 cm^{-1} corresponds to the O–H group stretching vibration. The weak peaks positioned at 3 065.74 and 3 002.37 cm^{-1} shifted to 2 931.55 and 2 860.73 cm^{-1}, respectively, indicate C–H group stretching. The peak at 1 606.48 cm^{-1} shifted to 1 636.30 cm^{-1} corresponds to the C=C stretching of the alkene group, and the sharp peak at 1 162.92 cm^{-1} shifted to 1 010.11 cm^{-1} is attributed to the C–O stretching. The absorption peaks that displayed shifts are assumed to be due to the TRPIDC-CH_3CdQDs formation, accomplished by the presence of various flavonoids, alkaloids, terpenoids, and other biopolymeric agents in the *M. oleifera* leaf extract. Shivaji et al. and Kandasamy et al. reported similar results using fruit sap and tea leaves, respectively [29, 40]

Morphology and particle size analysis

The HR-TEM image of TRPIDC-CH_3CdSQDs presented in Fig. 2(c) confirmed the structure and size of the QDs. The morphology displays the spherical

Table 2 Characteristics of phytochemicals found in *M. oleifera* leaf extract

Compound class	Phytochemical test	Literature	Ref.
Flavonoids	++	+	[36–39]
Alkaloids	++	+	[36–39]
Terpenoids	++	+	[36, 37, 39]

Note: ++ positive current study; + literature.

Table 3 Phytochemical analysis of the *M. oleifera* leaf extract.

Phytochemical analysis	Wavelength (nm)	Content	Dilution factor	Actual content
Phenolic content (mgTAE/g of extract)	750	57	5	285
Flavonoid content (mgQE/g of extract)	510	138	5	690
Total alkaloid content (mgAE/g of extract)	470	78	0	78

Note: QE, quercetin equivalent; TAE, tannic acid equivalent; AE, atropine equivalent.

particles with a size distribution of 3–9 nm and an average diameter of 4.5 nm (Fig. 2(d)) and the formation of a QD (< 10 nm) [40]. The non-homogeneity of the particle size may be attributed to QD agglomeration. The findings are consistent with previous studies on the use of plant extracts to synthesize CdSQDs. Borovaya et al. obtained spherical CdSQDs of predominantly 4–5 nm [17]. Shivaji et al. synthesized CdSQDs using tea leaves and obtained a range of 2–5 nm in particle size [29].

Cytotoxicity assay

The cytotoxicity effects of TRPIDC-CH_3CdSQDs against MCF-7, A549, and HEK923 cells were determined by the MTT assay. To determine how they influenced cell viability and proliferation, the cytotoxicity of QDs in a cancer cell line was examined. The cytotoxicity percentage of the QDs was investigated at 100 and 50 μg·mL^{-1} (Table 4). The average absorbance readings were determined according to the negative solvent regulation (at 1% DMSO), and all experiments were performed in triplicate. An overall low cytotoxic effect of the synthesized QDs against MCF-7, A549, and HEK293 cells was observed, with the highest activity percentage being against MCF-7 (63.8% ± 0.005%). Although the overall cytotoxicity was minimal, a dose-dependent increase in cytotoxic activity was observed as the concentration rose from 50 to 100 μg·mL^{-1}.

Table 4 Cytotoxicity of TRPIDC-CH_3CdSQDs against MCF-7, A549, and HEK293 cells.

	Cytotoxicity (%)	
Cells	μg·mL^{-1}	50 μg·mL^{-1}
MCF-7	63.8 ± 0.005^{ay}	49.1 ± 0.013^{bx}
A549	43.7 ± 0.15^{cy}	29.4 ± 0.03^{dx}
HEK293	2.3 ± 0.007^{ey}	0.25 ± 0.003^{fx}

Notes: Values are presented as mean ± SD. Means of growth inhibition without a common letter differ significantly ($p < 0.05$). a, b, c, d, e, and f indicate differences per row; x and y indicate differences between different concentrations.

The results are comparable to those of Shaheen et al., who reported the cytotoxic activity of GO-ZnO nanocomposites using the MTT assay against MCF-7 cells. Various concentrations were used (10–100 μg·mL^{-1}), and the cell viability was decreased to 90%, 79%, 62%, 55%, 47%, and 37% for MCF-7 cells at 10, 20, 40, 60, 80, and 100 μg·mL^{-1}, respectively [42]. El-Sayed et al. synthesized a culture extract of *Monascus purpureus* ATCC16436 grown on sugarcane bagasse under solid-state fermentation and assessed their anticancer activity against MCF-7, HepG2, and normal NHEM cell lines. Their results indicated that the synthesized samples are less toxic against normal cells [43].

The microscopy analysis looked at the morphological properties of untreated or treated cells. The control cells emerged in regular form and were attached to the surface. However, MCF-7 cells, which were exposed to TRPIC-CH_3CdSQDs and lost their normal form and ability to bind cells, decreased in cell density (Fig. 3). Such alterations have also been reported using plant-synthesized AgNPs in different cancer cell lines [44], indicating that the cytotoxic effect of synthesized TRPIC-CH_3CdSQDs could be due to their antineoplastic properties and their ability to cause cell death by multiple molecular mechanisms [45].

Protein interaction studies

UV–Vis absorption studies

UV–Vis absorption is a simple and relevant measurement used to study structural changes and prove complex formations. A strong absorption band at around 278 nm, which was primarily due to the π→π* transition [33], was observed (Fig. 4(a)). The absorbance of this peak is mainly due to the absorption of tryptophan [34, 46], and it increases gradually with the TRPIDC-CH_3CdSQD

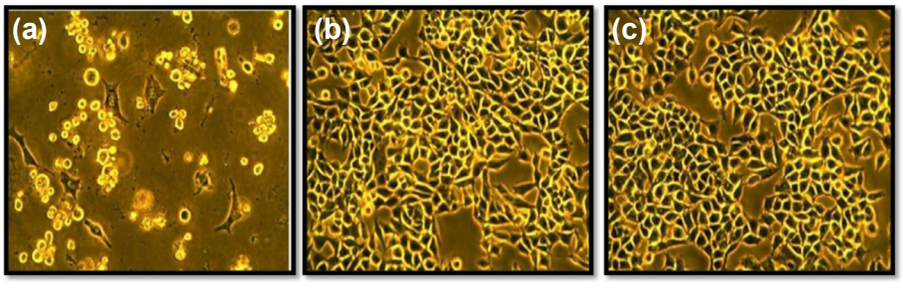

Fig. 3 Morphology of MCF-7 cells (100× magnification) treated with **(a)** CH_3CdSQDs, **(b)** DMSO (1%), or **(c)** untreated.

concentration, without any shift in the peak position. These observations indicate a structural change (micro-environment) in HSA and the formation of a ground-state complex between HSA and TRPIDC-CH_3CdSQDs [32, 33]. Figure 4(b) indicates the linear fits of increasing TRPIDC-CH_3CdQD concentrations at 278 nm, confirming the positive correlation between TRPIDC-CH_3CdQD concentrations and the complex formation. Equations (5) and (6) were used to measure the degree of complex forming between HSA and TRPIDC-CH3CdSQDs. According to the Benesi-Hildebrand relationship equation, the binding constant of complex formation was calculated from the shift in intensity of the absorption peak at 278 nm (Eq. (1)). From the plot slope of $1/(A - A_0)$ vs.$1/[Q]$ (Fig. 4(c)), K_b was measured, and its value was 1.76×10^2 M^{-1}.

$$\text{HSA} + \text{TRPIDC-CH}_3\text{CdSQDs} \underset{K_b}{} \text{HSA}\ldots\ldots \text{TRPIDC-CH}_3\text{CdSQDs} \quad (5)$$

$$K_b = \frac{[\text{HSA}\ldots\ldots\text{TRPIDC-CH}_3\text{CdSQDs}]}{[\text{HSA}] \times [\text{TRPIDC-CH}_3\text{CdSQDs}]} \quad (6)$$

Fluorescence quenching studies

The fluorescence spectral method was used to get more insight into the nature of the binding interaction of QDs with HAS. Three fluorophores are present in HAS: tryptophan, tyrosine, and phenylalanine. HSA fluorescence is mainly due to tryptophan alone because phenylalanine has a very low fluorescence quantum yield, and the fluorescence of tyrosine is almost totally quenched if it is ionized or near an amino group, a carboxyl group, or a tryptophan residue [33, 47]. Thus, the HSA intrinsic fluorescence is due mainly to the tryptophan residue in the hydrophobic cavity of subdomain IIA (Sudlow I). The HSA fluorescence emission spectra at various CH_3CdSQD concentrations with an excitation of 280 nm are seen in Fig. 5(a). The HSA fluorescence intensities decreased markedly with increased CH_3CdSQD concentrations, and no peak changes or new peaks were observed (Fig. 5(b)).

These findings indicate that the TRPIDC-CH_3CdSQD and HSA complex formed is responsible for quenching. Many molecular interactions, such as excited-state reactions, molecular rearrangements, energy transfer, ground-state complex forming, and collision quenching, may reduce the fluorescence strength of a compound, which is called fluorescence quenching [47]. Dynamic quenching refers to a phase in which fluorophore and quencher come into contact during the life of the excited state, whereas static

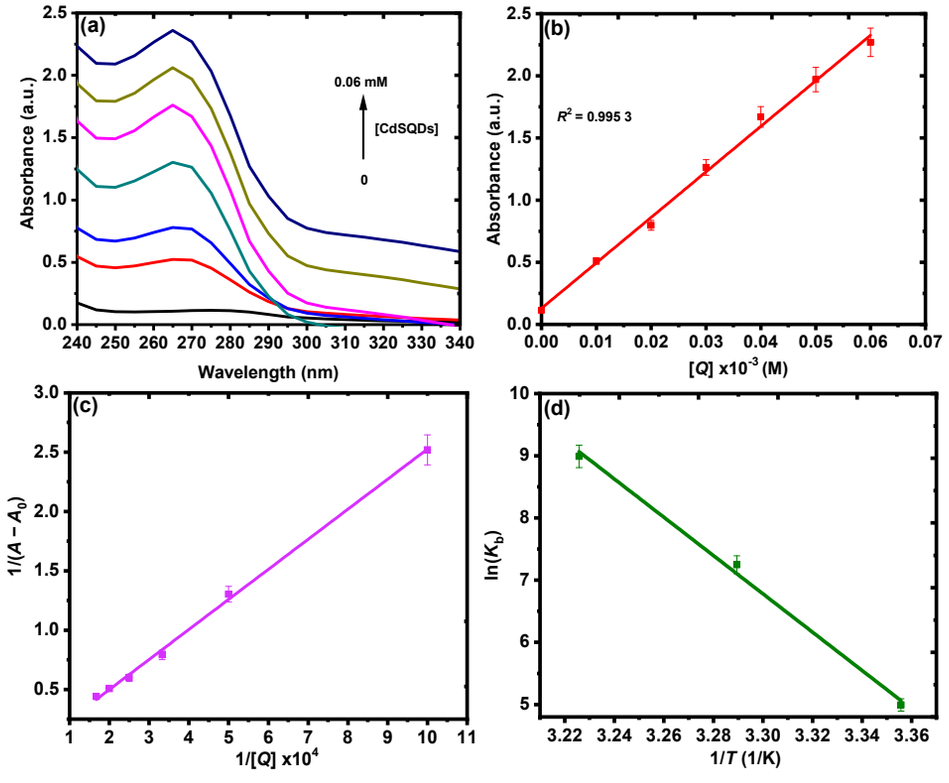

Fig. 4 (a) Absorbance spectra of HSA upon adding TRPIDC-CH_3CdSQDs. **(b)** Linear fit. **(c)** Plot of $1 / (A - A_0)$ versus $1/[Q]$. **(d)** Van't Hoff plot of HSA-TRPIDC-CH_3 CdSQDs.

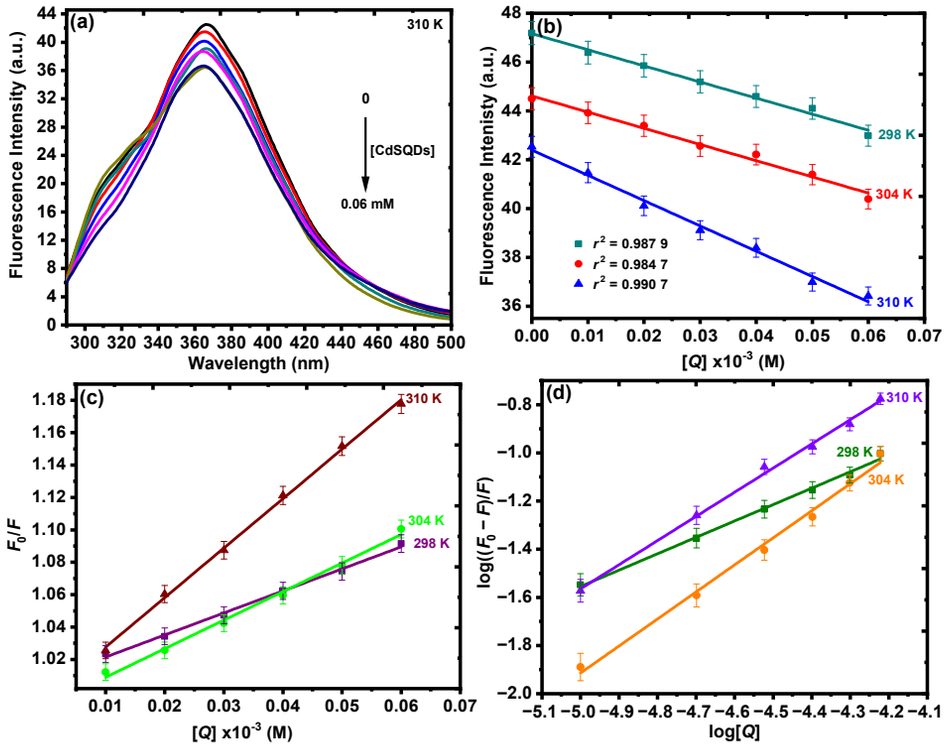

Fig. 5 Fluorescence quenching data for the HSA-TRPIDC-CH_3CdSQDs complex **(a)** Fluorescence spectrum of different TRPIDC-CH_3CdSQD concentrations. **(b)** Linear fit of the absorbance complex with increasing TRPIDC-CH_3CdSQD concentrations at 345 nm and different temperatures. **(c)** Stern–Volmer curves at different temperatures. **(d)** log[$(F_0 - F)/F$] vs. log[Q] plots at different temperatures.

quenching refers to the fluorophore-quencher complex formation. The fluorescence quenching process can be quantitatively evaluated at various temperatures using the Stern–Volmer equation (Eq. (2a)). Fig. 5(c) displays the Stern–Volmer plots of F_0/F vs. [Q] at three different temperatures (298, 304, and 310 K). The K_{SV} and K_q values were determined by the slope with τ_0~10^{-8} s (Table 5).

The fluorescence quenching mechanisms can be differentiated by their different dependence on temperature. The quenching constants decrease with the increase in temperature for static quenching, and the reverse effect is observed for dynamic quenching [32]. The K_{SV} and K_q values increased with the rise in temperature, suggesting that the quenching of the HSA-TRPIDC-CH_3CdSQDs system is dynamic. The binding constant (K_b) and the number of binding sites between TRPIDC-CH_3CdSQDs and HSA were calculated according to the double logarithm (Eq. (2b)). Figure 5(d) displays the double-logarithm curve, and Table 5 presents the corresponding measured results. The number of binding sites (n) is roughly 1 for all temperatures, suggesting one type of binding site. This result implies that the structural changes in HSA induced by TRPIDC-CH_3CdSQDs did not decrease its ability to bind with TRPIDC-CH_3CdSQDs, and the distances between the TRPIDC-CH_3CdSQDs and HAS binding site became profound [33].

Modes of binding

Most biological molecules bind with smaller molecules through interactions like hydrogen bonding, van der Waals forces, electrostatic, or hydrophobic and hydrophilic interactions [33]. Determining the change in entropy (ΔS) and enthalpy (ΔH) of a binding reaction can help determine the type of interactive forces. These parameters can be obtained by the van't Hoff and Gibbs free energy equations (Eqs. (3) and (4)) [33]. The HAS binding constant was determined at three different temperatures. The plot of lnK_b vs $1/T$ was plotted linearly to obtain the ΔH and ΔS values from the slope and the intercept, respectively (Fig. 4(d)). The ΔG of the reaction was determined using the ΔH and ΔS values (Table 6). The positive sign of ΔH and the negative sign of ΔG indicate that the binding mechanism is endothermic and spontaneous. The positive signs of ΔH and ΔS suggest the presence of hydrophobic interactions in the HSA-TRPIDC-

Table 5 The K_{SV}, K_q, $K_{b,}$ and n values of the HSA-TRPIDC-CH_3CdSQD complex

T (K)	K_{sv} (10^3 M^{-1})	K_q (10^{11} $M^{-1}\cdot S^{-1}$)	r^2	K_b (M^{-1})	n	r^2
298	1.36	1.36	0.995	7.03×10^2	0.68	0.992
304	1.76	7.82	0.992	2.83×10^3	1.00	0.996
310	3.05	3.05	0.998	5.02×10^3	1.12	0.995

Table 6 Thermodynamic parameters of the HSA–QD interaction

Parameters	Values
ΔH (kJ·mol^{-1}·K^{-1})	256.10
ΔS (kJ·mol^{-1}·K^{-1})	0.901
ΔG(kJ·mol^{-1}·K^{-1})	−12.40
Forces	Hydrophobic interactions

CH_3CdSQDs complex, according to the thermodynamic data [33, 47, 48].

Conclusion

The TRPIDC-CH_3CdSQDs were successfully synthesized using *M. oleifera* leaf extract and indole pyrazole ligand. The UV–Vis spectrum revealed a broad absorption band at 420 nm. The HR-TEM study confirmed the development of spherical QDs, which are nonhomogeneous in particle size due to agglomeration, with an average diameter of 4.5 nm. The synthesized QDs had a low cytotoxic effect on MCF-7, A549, and HEK293 cells, with a maximum activity percentage of 63. 8% ± 0.005% against MCF-7 cells at 100 μg·mL^{-1}. For the interaction studies, the increasing UV–Vis absorption spectra indicated that TRPIC-CH_3CdSQDs formed a ground-state complex with HSA. The decreasing fluorescence intensity revealed an increased quenching and a binding between HSA and TRPIC-CH_3CdSQDs at different temperatures. Thermodynamic parameters indicated that the forces of hydrophobic interactions played a major role in the interaction between TRPIC-CH_3CdSQDs and HSA. These QDs have the potential to be used in biological applications, such as drug delivery.

CRediT Author Statement

All authors contributed equally to this project.

Acknowledgements

The authors would like to extend their gratitude to the National Research Foundation (NRF) (MND190408428189) for their financial assistance

Conflict of Interests

The authors declare that they have no established competitive interests that may have had a bearing on the work stated in this article

Supporting Information

Supporting information to this article can be found online at http://doi.org/10.26599/NBE.2024.9290077

References

[1] J. Rajangam, P. Sampathi, N.N. Palei, et al. Green synthesis, characterization and antiepileptic activity of herbal nanoparticles of *Mimusops elengi* in mice. *Nano Biomedicine and Engineering*, 2022, 14(4): 295−307. https://doi.org/10.5101/nbe.v14i4.p295-307

[2] B.A. de Marco, B.S. Rechelo, E.G. Tótoli, et al. Evolution of green chemistry and its multidimensional impacts: A review. *Saudi Pharmaceutical Journal*, 2019, 27(1): 1−8. https://doi.org/10.1016/j.jsps.2018.07.011

[3] P. Rauwel, S. Küünal, S. Ferdov, et al. A review on the green synthesis of silver nanoparticles and their morphologies studied via TEM. *Advances in Materials Science and Engineering*, 2015, 2015: 682749. https://doi.org/10.1155/2015/682749

[4] Z. Machalova, M. Sajfrtova, R. Pavela, et al. Extraction of botanical pesticides from *Pelargonium graveolens* using supercritical carbon dioxide. *Industrial Crops and Products*, 2015, 67: 310−317. https://doi.org/10.1016/j.indcrop.2015.01.070

[5] V.V. Makarov, A.J. Love, O.V. Sinitsyna, et al. "Green" nanotechnologies: Synthesis of metal nanoparticles using plants. *Acta Naturae*, 2014, 6(1): 35–44. https://doi.org/10.32607/20758251-2014-6-1-35-44

[6] A.C. Mendes Hacke, D. Lima, S. Kuss. Green synthesis of electroactive nanomaterials by using plant-derived natural products. *Journal of Electroanalytical Chemistry*, 2022, 922: 116786. https://doi.org/10.1016/j.jelechem.2022.116786

[7] E. Alzahrani, A.T. Alkhudidy. Synthesis, optimization, and characterization of ecofriendly production of gold nanoparticles using lemon peel extract. *International Journal of Analytical Chemistry*, 2021, 2021: 7192868. https://doi.org/10.1155/2021/7192868

[8] A.T. Oyeyinka, S.A. Oyeyinka. *Moringa oleifera* as a food fortificant: Recent trends and prospects. *Journal of the Saudi Society of Agricultural Sciences*, 2018, 17(2):

127–136. https://doi.org/10.1016/j.jssas.2016.02.002
[9] B.B. Zhao, T. Lan, H. Li, et al. Antioxidation activity of *Moringa oleifera* Lam. leaves extract on soybean oil during both storage and thermal treatment. *Journal of Food Processing and Preservation*, 2019, 43(8): e13975. https://doi.org/10.1111/jfpp.13975
[10] C. Tiloke, A. Phulukdaree, R.M. Gengan, et al. *Moringa oleifera* Aqueous leaf extract induces cell-cycle arrest and apoptosis in human liver hepatocellular carcinoma cells. *Nutrition and Cancer*, 2019, 71(7): 1165–1174. https://doi.org/10.1080/01635581.2019.1597136
[11] K. El-bakry, E.-s. Toson, M. Serag, et al. Hepatoprotective effect of *Moringa oleifera* leaves extract against carbon tetrachloride-induced liver damage in rats. *World journal of pharmaceutical research*, 2016, 5(5): 76−89.
[12] D.E. Pratiwi, S. Side , N.A.T. Nisa. Synthesis of silver nanoparticles using *Moringa oleifera* L. leaf extract as bioreductor. In: Proceedings of the 1st International Symposium on Green Materials and Technology, 2018: 145–149. https://doi.org/10.4028/www.scientific.net/MSF.967.145
[13] J. Seetha, U.M. Mallavarapu, P. Akepogu, et al. Biosynthesis and study of bimetallic copper and silver nanoparticles on cellulose cotton fabrics using *Moringa oliefiera* leaf extraction as reductant. *Inorganic and Nano-Metal Chemistry*, 2020, 50(9): 828−835. https://doi.org/10.1080/24701556.2020.1725571
[14] N. Matinise, X.G. Fuku, K. Kaviyarasu, et al. ZnO nanoparticles via *Moringa oleifera* green synthesis: Physical properties & mechanism of formation. *Applied Surface Science*, 2017, 406: 339−347. https://doi.org/10.1016/j.apsusc.2017.01.219
[15] G.D. Reddy, M. Noorjahan, K.G. Mangatayaru, et al. Microwave assisted phytosynthesis and characterization of magnetic iron oxide quantum dots using *Moringa oleifera*. *Material Science Research India*, 2018, 15(2): 145–150. https://doi.org/10.13005/msri/150206
[16] E. Kalugendo, P. Kousalya. Synthesis of silver nanoparticles using *Moringa oleifera* seeds, *Glycyrrhiza glabra* stems, and its anti-methicillin-resistant *Staphylococcus aureus* activity. *Asian Journal of Pharmaceutical and Clinical Research*, 2019, 12(2): 368−370. https://doi.org/10.22159/ajpcr.2019.v12i2.28863
[17] M. Borovaya, Y. Pirko, T. Krupodorova, et al. Biosynthesis of cadmium sulphide quantum dots by using *Pleurotus ostreatus* (Jacq.) P. Kumm. *Biotechnology & Biotechnological Equipment*, 2015, 29(6): 1156−1163. https://doi.org/10.1080/13102818.2015.1064264
[18] Z.J. Qin, Q.L. Yue, Y. Liang, et al. Extracellular biosynthesis of biocompatible cadmium sulfide quantum dots using *Trametes versicolor*. *Journal of Biotechnology*, 2018, 284: 52–56. https://doi.org/10.1016/j.jbiotec.2018.08.004
[19] H. Mohd Yusof, N. Abdul Rahman, R. Mohamad, et al. Microbial mediated synthesis of silver nanoparticles by *Lactobacillus plantarum* TA4 and its antibacterial and antioxidant activity. *Applied Sciences*, 2020, 10(19): 6973. https://doi.org/10.3390/app10196973
[20] G. Gahlawat, A.R. Choudhury. A review on the biosynthesis of metal and metal salt nanoparticles by microbes. *RSC Advances*, 2019, 9(23): 12944−12967. https://doi.org/10.1039/C8RA10483B
[21] D. Verma, N. Gulati, S. Kaul, et al. Protein based nanostructures for drug delivery. *Journal of Pharmaceutics*, 2018, 2018: 9285854. https://doi.org/10.1155/2018/9285854
[22] J.M. Jacob, S. Sharma, R.M. Balakrishnan. Exploring the fungal protein cadre in the biosynthesis of PbSe quantum dots. *Journal of Hazardous Materials*, 2017, 324: 54−61. https://doi.org/10.1016/j.jhazmat.2015.12.05
[23] Z. Al-Shalabi, P.M. Doran. Biosynthesis of fluorescent CdS nanocrystals with semiconductor properties: Comparison of microbial and plant production systems. *Journal of Biotechnology*, 2016, 223: 13−23. https://doi.org/10.1016/j.jbiotec.2016.02.018
[24] G.R. Bardajee, Z. Hooshyar. Interaction of a novel starch-capped CdS quantum dots with human serum albumin and bovine serum albumin. *Starch*, 2016, 68(3-4): 329−338. https://doi.org/10.1002/star.201500092
[25] T.R. Makhanya, R.M. Gengan, K. Kasumbwe. Synthesis of fused indolo-pyrazoles and their antimicrobial and insecticidal activities against *Anopheles arabiensis* mosquito. *ChemistrySelect*, 2020, 5(9): 2756−2762. https://doi.org/10.1002/slct.201904620
[26] S. Dadiboyena, A. Nefzi. Synthesis of functionalized tetrasubstituted pyrazolyl heterocycles–A review. *European Journal of Medicinal Chemistry*, 2011, 46(11): 5258−5275. https://doi.org/10.1016/j.ejmech.2011.09.016
[27] S. Baliyan, R. Mukherjee, A. Priyadarshini, et al. Determination of antioxidants by DPPH radical scavenging activity and quantitative phytochemical analysis of *Ficus religiosa*. *Molecules*, 2022, 27(4): 1326. https://doi.org/10.3390/molecules27041326
[28] C. Otitolaiye, A. Omonkhua, K. Oriakhi, et al. Phytochemical analysis and *in vitro* antioxidant potential of aqueous and ethanol extracts of Irvingia gabonensis stem bark. *Pharmacognosy Research*, 2023, 15(2): 363−372. https://doi.org/10.5530/pres.15.2.039
[29] K. Shivaji, S. Mani, P. Ponmurugan, et al. Green-synthesis-derived CdS quantum dots using tea leaf extract: Antimicrobial, bioimaging, and therapeutic applications in lung cancer cells. *ACS Applied Nano Materials*, 2018, 1(4): 1683−1693. https://doi.org/10.1021/acsanm.8b00147
[30] X.Q. Wu, C. Huang, Y.M. Jia, et al. Novel coumarin-dihydropyrazole thio-ethanone derivatives: Design, synthesis and anticancer activity. *European Journal of Medicinal Chemistry*, 2014, 74: 717−725. https://doi.org/10.1016/j.ejmech.2013.06.014
[31] S. Majeed, M.S. bin Abdullah, A. Nanda, et al. *In vitro* study of the antibacterial and anticancer activities of silver nanoparticles synthesized from *Penicillium brevicompactum* (MTCC-1999). *Journal of Taibah University for Science*, 2016, 10(4): 614–620. https://doi.org/10.1016/j.jtusci.2016.02.010
[32] S. Prasanth, C. Sudarsanakumar. Elucidating the interaction of L-cysteine-capped selenium nanoparticles and human serum albumin: Spectroscopic and thermodynamic analysis. *New Journal of Chemistry*, 2017, 41(17): 9521−9530. https://doi.org/10.1039/c7nj00477j
[33] A.V. Pansare, A.A. Shedge, V.R. Patil. Discrete SeNPs-macromolecule binding manipulated by hydrophilic interaction. *International Journal of Biological Macromolecules*, 2018, 107: 1982−1987. https://doi.org/10.1016/j.ijbiomac.2017.10.065
[34] M. Mahanthappa, M.A. Savanur, B. Puthusseri, et al. Spectroscopic and electrochemical studies on the molecular interaction between copper sulphide nanoparticles and bovine serum albumin. *Journal of Materials Science*, 2018, 53(1): 202−214. https://doi.org/10.1007/s10853-017-1521-8
[35] I. Ocsoy, D. Tasdemir, S. Mazicioglu, et al. Nanotechnology in plants. In: Plant Genetics and Molecular Biology. Advances in Biochemical Engineering/Biotechnology, vol 164. R. Varshney, M. Pandey, A. Chitikineni, eds. Springer, 2018: 263–275. https://doi.org/10.1007/10_2017_53

[36] P. Ilanko, P.A. McDonnell, S. van Vuuren, et al. Interactive antibacterial profile of *Moringa oleifera* Lam. extracts and conventional antibiotics against bacterial triggers of some autoimmune inflammatory diseases. *South African Journal of Botany*, 2019, 124: 420−435. https://doi.org/10.1016/j.sajb.2019.04.008

[37] P.E. Das, I.A. Abu-Yousef, A.F. Majdalawieh, et al. Green synthesis of encapsulated copper nanoparticles using a hydroalcoholic extract of *Moringa oleifera* leaves and assessment of their antioxidant and antimicrobial activities. *Molecules*, 2020, 25(3): 555. https://doi.org/10.3390/molecules25030555

[38] S. Suresh, A.S. Chhipa, M. Gupta, et al. Phytochemical analysis and pharmacological evaluation of methanolic leaf extract of *Moringa oleifera* Lam. in ovalbumin induced allergic asthma. *South African Journal of Botany*, 2020, 130: 484−493. https://doi.org/10.1016/j.sajb.2020.01.046

[39] P. Srivastava, G. Srivastava. Pharmacological and phytochemical screening of *Desmodium gangeticum* and *Moringa oleifera*. *Research Journal of Chemistry and Environment*, 2018, 22(5): 6–10.

[40] K. Kandasamy, M. Venkatesh, Y.A. Syed Khadar, et al. One-pot green synthesis of CdS quantum dots using *Opuntia ficus-indica* fruit sap. *Materials Today: Proceedings*, 2020, 26: 3503−3506. https://doi.org/10.1016/j.matpr.2019.06.003

[41] G.B. Jegadeesan, K. Srimathi, N. Santosh Srinivas, et al. Green synthesis of iron oxide nanoparticles using *Terminalia bellirica* and *Moringa oleifera* fruit and leaf extracts: Antioxidant, antibacterial and thermoacoustic properties. *Biocatalysis and Agricultural Biotechnology*, 2019, 21: 101354. https://doi.org/10.1016/j.bcab.2019.101354

[42] F. Shaheen, M. Aziz, M. Fatima, et al. *In vitro* cytotoxicity and morphological assessments of GO-ZnO against the MCF-7 cells: Determination of singlet oxygen by chemical trapping. *Nanomaterials*, 2018, 8(7): 539. https://doi.org/10.3390/nano8070539

[43] E.SR. El-Sayed, H.K. Abdelhakim, A.S. Ahmed. Solid-state fermentation for enhanced production of selenium nanoparticles by gamma-irradiated *Monascus purpureus* and their biological evaluation and photocatalytic activities. *Bioprocess and Biosystems Engineering*, 2020, 43(5): 797−809. https://doi.org/10.1007/s00449-019-02275-7

[44] R. Vivek, R. Thangam, K. Muthuchelian, et al. Green biosynthesis of silver nanoparticles from *Annona squamosa* leaf extract and its *in vitro* cytotoxic effect on MCF-7 cells. *Process Biochemistry*, 2012, 47(12): 2405−2410. https://doi.org/10.1016/j.procbio.2012.09.025

[45] M.A. Farah, M.A. Ali, S.M. Chen, et al. Silver nanoparticles synthesized from *Adenium obesum* leaf extract induced DNA damage, apoptosis and autophagy via generation of reactive oxygen species. *Colloids and Surfaces B*: *Biointerfaces*, 2016, 141: 158−169. https://doi.org/10.1016/j.colsurfb.2016.01.027

[46] M. Ishtikhar, G. Rabbani, S. Khan, et al. Biophysical investigation of thymoquinone binding to 'N' and 'B' isoforms of human serum albumin: Exploring the interaction mechanism and radical scavenging activity. *RSC Advances*, 2015, 5(24): 18218−18232. https://doi.org/10.1039/c4ra09892g

[47] G. Rezanejade Bardajee, Z. Hooshyar, M. Rezaei, et al. Spectroscopic studies on the interactions of capped CdS quantum dots with human serum albumin (HSA) and bovine serum albumin (BSA). *Inorganic and Nano-Metal Chemistry*, 2017, 47(5): 688−696. https://doi.org/10.1080/15533174.2016.1186098

[48] S. Devi, S. Tyagi. Fluorescent determination of trinitrotoluene with bovine serum albumin mediated enhancement of thioglycolic acid capped cadmium selenium quantum dots. *Instrumentation Science & Technology*, 2019, 47(3): 292−311. https://doi.org/10.1080/10739149.2018.1531019